ELSEVIER

Journal of Nuclear Materials 245 (1997) 152–160

journal of nuclear materials

High pressure oxidation of sponge-Zr in steam/hydrogen mixtures

Yeon soo Kim [a,*], Wei-E Wang [a], Soo Lim [a], D.R. Olander [a], S.K. Yagnik [b]

[a] *Department of Nuclear Engineering, University of California, Berkeley, CA 94720, USA*
[b] *Electric Power Research Institute, Palo Alto, CA 94303, USA*

Received 12 November 1996; accepted 11 February 1997

Abstract

A thermogravimetric apparatus for operation in 1 and 70 atm steam–hydrogen or steam–helium mixtures was used to investigate the oxidation kinetics of sponge-Zr containing 215 ppm Fe. Weight-gain rates, reflecting both oxygen and hydrogen uptake, were measured in the temperature range 350–400°C. The specimens consisted of thin sponge-Zr layers metallurgically bonded to a Zircaloy disk. The edges of the disk specimens were coated with a thin layer of pure gold to avoid the deleterious effect of corners. Following each experiment, the specimens were examined metallographically to reveal the morphology of the oxide and/or hydride formed. Two types of oxide, one black and uniform and the other white and nodular, were observed on sponge-Zr surfaces oxidized in steam environments at 70 atm. The oxidation rate when white-nodular oxide formed was a factor of two higher than that of black-uniform oxide at 400°C for steam contents above 1 mol%. The oxidation rate was independent of total pressure, the carrier gas (H_2 or He) and steam content above ~ 1 mol%. The oxidation kinetics of sponge-Zr follows a linear law for maximum reaction times up to ~ 6 days. The oxidation rate in steam–hydrogen mixtures at 70 atm total pressure decreases when the steam content approaches the steam-starved region (~ 0.5 mol% steam at 400°C and ~ 0.02 mol% steam at 350°C). Lower steam concentrations cause massive hydriding of the specimens. Even at steam concentrations above the critical value, direct hydrogen absorption from the gas was manifest by hydrogen pickup fractions greater than unity.

1. Introduction

1.1. Motivation for the investigation

Extended burnup operation of LWR fuel requires sound performance of the inner as well as the outer surfaces of the cladding. The chemical behavior of the inner surface is of concern because it determines the life of cladding in defective fuel rods. The gap in a defective fuel rod is initially filled with superheated steam and helium. As the inner surface of cladding oxidizes, hydrogen buildup in the gas enhances hydrogen ingress to the cladding, which may lead to secondary hydriding. A detailed chemistry-transport analysis of the processes occurring in the gap of a defective fuel rod is available in Ref. [1].

Although massive hydriding of the cladding, rather than inner-wall oxidation, is the ultimate cause of the severe cladding degradation, oxidation plays a critical role in the process for several reasons. First, steam corrosion of the inner wall produces the bulk of the hydrogen in the gap that leads to the steam-starved conditions necessary for hydriding to take place. The sponge-Zr liner on the Zircaloy (Zry), introduced a decade ago to prevent pellet-cladding interaction [2], oxidizes more rapidly than conventional Zry. The majority of the fuel rods that failed by massive hydriding have been of the liner type. The more easily oxidized sponge-Zr is believed to be the reason for the greater propensity of failed rods to degrade further by massive hydriding. For this reason, the oxidation behavior of sponge-Zr is the focus of the present investigation. Second, the morphology and thickness of the oxide formed on the liner surface of a failed rod affects the resistance of the metal to hydrogen absorption. Third, in steam-starved conditions near the critical H_2/H_2O ratio for massive

* Corresponding author. Tel.: +1-510 642 7158; fax: +1-510 643 9685; e-mail: yskim@nuc.berkeley.edu.usa.

PII S0022-3115(97)00018-4

hydriding, both oxidation and hydriding occur simultaneously.

1.2. Previous investigation of zr oxidation in steam

Oxidation of zirconium and Zircaloy has been extensively studied during the past decades. However, the majority of early studies were concerned with oxidation of Zr by oxygen [3] and recent studies have concentrated mostly on waterside corrosion of Zircaloy cladding [4–9]. Several works have reported on zirconium oxidation in steam environments but these were at atmospheric pressure or below [10–15]. Numerous studies dealt with elevated-pressure oxidation of zirconium in steam or steam–gas mixtures at around 400°C [16–22]. Seibold et al. [23] reported the effect of Fe content on oxidation of sponge-Zr in 1 atm steam. They showed that pure zirconium liner has poor resistance to steam corrosion whereas improved resistance can be achieved by adding 0.3–0.4% iron by weight.

Observations of the total-pressure dependence of zirconium oxidation reported in the literature are summarized in Table 1. Wanklyn [17] and Cox [18] agree that the pressure dependence decreases as the corrosion resistance of the alloy improves. Results from Refs. [19,20] are also concordant with those of Refs. [17,18] for Zircaloy oxidation. For comparison, the present work did not observe a variation in the corrosion rate of sponge-Zr with either steam total pressure or steam partial pressure.

1.3. Scope of the study

The present paper reports results obtained during oxidation tests of sponge-Zr in high pressure hydrogen or helium gas containing 0.1–20% steam at 350–400°C. Most experiments were conducted at 70 atm because this is the gas pressure experienced be the cladding inner surface in failed BWR fuel rods. Some 1 atm runs were conducted to investigate the total pressure effect on oxidation kinetics.

Table 1
Pressure dependence of crystal-bar Zr and Zry corrosion in steam and oxygen at ~ 400°C

Gas\metal	Crystal-bar Zr	Zry
Wanklyn et al. [17]		
O_2	none	none
H_2O	large	small
Cox [18]		
H_2O	large	none
Shannon [20]		
H_2O	–	none
Johnson [21]		
H_2O	–	none

The principal method of measuring oxidation kinetics was in-situ weight-gain determination by a continuously-recording microbalance operating in the high-pressure system. Subsidiary measurements included microscopic examination of the oxide and hydride morphology and hydrogen-content determination of the reacted specimens by the gas-extraction method.

2. Experimental

In-situ measurements of specimen weight in the high-pressure system were initially accomplished using a continuously-recording thermogravimetric apparatus (TGA). The early-version TGA system used two carrier gas lines supplied by a common gas cylinder: one for purging the microbalance chamber, the other for bubbling through water in a saturator to produce the desired steam contents. The gas lines joined at a tee just before flowing through the specimen chamber and exiting from the system. The steam content of the gas mixture was controlled by the saturator temperature. The main disadvantages of this TGA version were:

(i) The long time to obtain the equilibrium steam content in the specimen chamber.

(ii) The long steam-gas mixture line to be heated above the saturation temperature to avoid condensation.

(iii) The higher flow resistance of the gas line through the saturator than the line through the microbalance chamber. This could lead the saturator to retain a small amount of residual hydrogen from previous hydrogen–steam mixture tests.

The final-version TGA shown in Fig. 1 has been in use in the majority of experimental runs. The system operates at 70 atm and 350–400°C of steam–hydrogen or steam–helium gas mixtures. The specimen chamber is vertically connected to the microbalance chamber by the hangdown tube. The microbalance chamber is placed on a steel frame. The steam inlet leg is connected in the middle of the hangdown tube. The desired steam content in the high-pressure-gas-flow stream is achieved by using a direct liquid water feed that flashes into steam upon entering the flowing carrier gas (H_2 or He) at the entry to the specimen chamber. Constant water flow is provided by the Liqui-Flow™ unit made by the Porter Instrument Company. This equipment controls and measures water flows from 0.01 to 10 g/h in the high pressure line. Direct water feed (as opposed to saturating the carrier gas by bubbling through a liquid reservoir in the early TGA version) eliminates the difficulties cited above. To prevent ingress of the corrosive steam from the specimen chamber into the microbalance chamber, the high pressure carrier gas flows first through the microbalance chamber, then via the hangdown tube, through the specimen chamber before exiting at the bottom of the specimen chamber. The specimen chamber is 50 mm long and 16 mm inside diameter.

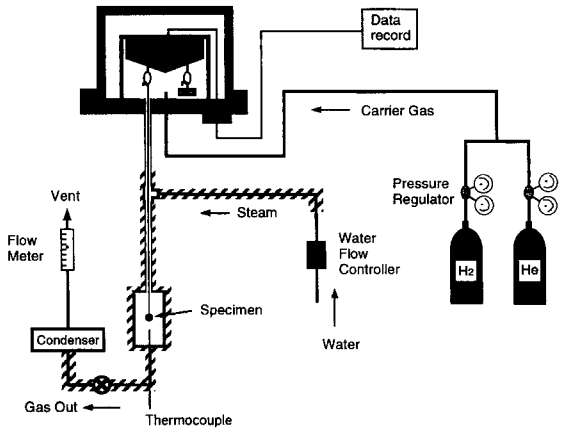

Fig. 1. Schematic diagram of high-pressure thermobalance system. The hatched lines are heated by heating tapes to prevent steam condensation.

Two types of experiments were performed. The batch-specimen experiment uses up to five specimens simultaneously, with the before-and-after weight gains determined for each by a table-top microbalance that measures weights with an accuracy of ~ 10 μg. The single-specimen experiment uses one specimen whose weight gain history is recorded in situ by the TGA. Although the in-situ microbalance has the same accuracy as the table-top version, other distortions of the signal are observed. On beginning an experiment, there is usually a transient period lasting up to several hours during which the microbalance output stabilizes. This is most likely due to establishment of a steady temperature in the apparatus. Additionally, in a flowing gas system, the apparent weight is affected by temperature and total pressure fluctuations and by flow-induced vibrations. Of particular importance is natural convection induced by the unstable gas-density distribution inherent in the method (cold gas in the microbalance chamber on top of the hot gas in the specimen chamber). The method of dealing with these problems has been considered in detail in Ref. [24]. Weight gains of the order of 50–100 μg are considered necessary for acquisition of reliable data from the TGA.

Commercial-grade hydrogen and helium were used as carrier gases. The impurities of concern in the gas used in hydriding experiments are oxygen and water vapor because they control the oxidant-to-hydrogen ratio. The impurity contents of hydrogen gas are 10 ppm O_2 and 5 ppm H_2O. The helium contained ~ 1 ppm hydrogen. Carrier gas flow rates are 1–1.5 l/min.

Specimens are cut as 9 mm diameter disks from a specially-fabricated Teledyne Wah Chang plate of 1 mm thick Zry (Zircaloy-2) on which layers of ~ 75 μm thick sponge-Zr were co-extruded on both sides. This sponge-Zr-sandwiched Zry plate is labeled Zr/Zry/Zr. The impurity content of the sponge-Zr is given in Table 2. The sponge-Zr layer used in this study was fabricated by a process similar to that used for zirconium-lined cladding tube with two significant differences:

(i) The texture of plate-type rather than tube-Zry, which is not believed to be significant because the hydride platelets were observed to form parallel to the surface, as in unstressed tube material.

(ii) The Fe content of 0.02% by weight, which places this material in the region of rapid change in corrosion rate with iron content and poor corrosion resistance [23].

To avoid the experimental artifact of corners, the edges of the disk specimens are coated with a thin layer of gold by plasma deposition. Prior to gold coating, all specimens are abraded with 1200-grit sandpaper and pickled in a 50% H_2O + 45% HNO_3 + 5% HF solution for 2 min.

Two types of optical microscopic examinations are performed. The cross-section surface is prepared by polishing and subsequent etching with a 60% H_2O_2 + 39% HNO_3 + 1% HF solution for ~ 2 min. The surface directly exposed to the gas is examined after reaction without further processing.

In mixed H_2/H_2O reactant gases, both oxidation and hydriding can occur simultaneously. Consequently, the

Table 2
Zr ingot chemistry analysis

Element	Concentration in ppm
Al	< 20
B	< 0.25
C	35
Ca	< 10
Cd	< 0.25
Cl	5
Co	< 10
Cr	< 50
Cu	< 10
Fe	215
H	< 5
Hf	55
Mg	< 10
Mn	< 25
Mo	< 10
N	13
Na	< 5
Nb	< 50
Ni	< 35
O	435
P	6
Pb	< 25
Si	< 25
Sn	< 10
Ta	< 50
Ti	< 25
U	< 1.0
V	< 25
W	< 25

Table 3
Collection of oxidation reactions of Zr/Zry/Zr in 70 atm steam–helium mixtures at 400°C (from single-specimen tests)

Run No.	Steam content (%)	Reaction time (h)	Oxidation rate (mg/dm^2 s) $\times 10^{-4}$	Oxide type	Hydrogen content (ppm)	Pickup fraction [b]
OP31	2	50	5.4 [a]	white	278	1.48
OP35	2	57	1.4	black	–	–
OP36	2	62	0.8	black	–	–
OP119	2	25	7.2	white	50	0.37
OP32	5	62	2.2 [a]	black	117	1.23
OP33	5	49	2.2	black	–	–
OP37	5	35	1.3	black	–	–
OP34	10	23	4.3	black	–	–
OP38	10	38	1.1	black	–	–

[a] Corrected for hydrogen absorbed.
[b] Ratio of hydrogen absorbed to hydrogen produced by oxidation.

weight-gain rate provided by the TGA is not a unique measure of specimen reactivity. Therefore, a specially-built hydrogen analyzer is used to determine hydrogen content in the reacted specimens. The hydrogen analyzer uses the method of hot extraction of hydrogen absorbed in the specimen by heating the specimen in a closed system and measuring the pressure increase [25].

3. Results and discussion

Table 3 gives the collected results of oxidation in steam–helium mixtures at 400°C. All runs in this table were obtained from single-specimen experiments. Collected oxidation results in steam–hydrogen mixtures are given for 350°C in Table 4 and for 400°C in Table 5, respectively. The reason for not providing hydrogen content for all specimens is that some specimens were used in follow-on hydriding experiments.

3.1. Morphology of reacted specimens

3.1.1. Surface

Shown in Fig. 2 are photos of surface morphology of fresh specimens and specimens oxidized in steam–hydrogen mixtures at 400°C. These photos were taken from the disk surface without further processing of the specimens. For comparison, photo (a) is of the fresh sponge-Zr surface taken before the specimen is loaded into reaction chamber; photos (b) and (c) were taken after reaction. Photo (b) shows a white bumpy oxide surface (OP67). Distinct oxide nodules are visible in a white oxide. The white spots (visible to the naked eye) are attributed to these nodules reflecting light non-uniformly. The black oxide on the specimen shown in photo (c) does not have such nodules (OP65).

3.1.2. Cross-section

The oxide film obtained from Run OP62 with a 20% steam and 80% hydrogen mixture at 400°C for 47 h shows

Table 4
Collection of oxidation reactions of Zr/Zry/Zr in 70 atm steam–hydrogen mixtures at 350°C

Run No.	Steam content (%)	Reaction time (h)	Oxidation rate (mg/dm^2 s) $\times 10^{-4}$	Oxide type	Hydrogen content (ppm)	Pickup fraction [b]
OP109	0.1	108	0.5 [a]	white	304	7.81
OP108	0.5	24	0.8 [a]	white	184	13.67
OP103	3	69	1.3 [a]	white	132	1.81
OP116 [c]	3	17	1.4	black	–	–
OP71(#1) [d]	4	8	2.7 [a]	black	45	2.50
OP71(#2) [d]	4	8	5.4	black	–	–
OP65(#1) [d]	20	35	1.9 [a]	black	82	1.57
OP65(#2) [d]	20	35	2.1	black	–	–
OP65(#3) [d]	20	35	2.1	black	–	–

[a] Corrected for hydrogen absorbed.
[b] Ratio of hydrogen absorbed to hydrogen produced by oxidation.
[c] Pressure for this run is 2 atm.
[d] Batch experiment.

Table 5
Collection of oxidation reactions of Zr/Zry/Zr in 70 atm steam–hydrogen mixtures at 400°C

Run No. (%)	Steam content	Preoxide film (μm)	Reaction time (h)	Oxidation rate (mg/dm^2 s) × 10^{-4}	Oxide type	Hydrogen content (ppm)	Pickup fraction [b]
OP53	0.5	2.9	138	0.6 [a]	white	87	0.75
OP70	0.5	2.1	421	0.5 [a]	black	712	4.01
OP61P [c]	0.5 → 5	0	52	1.1	black	–	–
OP66	1	2.3	44	2.9 [a]	black	238	2.15
OP68	1	2.2	67	2.7 [a]	black	392	2.47
OP67	1	1.1	212	1.4 [a]	white	349	1.30
OP73	1	0	260	3.2 [a]	white	640	0.71
OP51	1.3	0	120	3.4	white	–	–
OP52	5	0	49	3.8 [a]	white	95	0.47
OP79(#1) [d]	6	0	3	6.4	white	–	–
OP79(#2) [d]	6	0	3	5.9	white	–	–
OP62(#1) [d]	20	0	47	7.0 [a]	white	140	0.43
OP62(#2) [d]	20	0	47	6.9	white	–	–
OP62(#3) [d]	20	0	47	5.0	white	–	–
OP62(#4) [d]	20	0	47	6.6	white	–	–

[a] Corrected for hydrogen absorbed.
[b] Ratio of hydrogen absorbed to hydrogen produced by oxidation.
[c] Gas changed from helium and 0.5% steam to hydrogen and 5% steam at 10 h.
[d] Batch experiment.

a fairly uniform oxide layer thickness of ~5 μm with some locally thicker oxidized spots (see Fig. 3). This figure shows hydride platelets parallel to the specimen surface deep inside the Zry substrate. Sponge-Zr layer does not appear to have hydrides, nor did hydride platelets form in the Zry adjacent to it.

Fig. 4 shows the cross-sectional morphology of the white oxide (OP67) that was oxidized in 1% steam and 99% hydrogen at 400°C and 70 atm for 212 h. Photo (a) was taken before etching the polished specimen. The white spots seen visually are revealed in the microscope to be nodular bumps approximately 250 μm in diameter. The

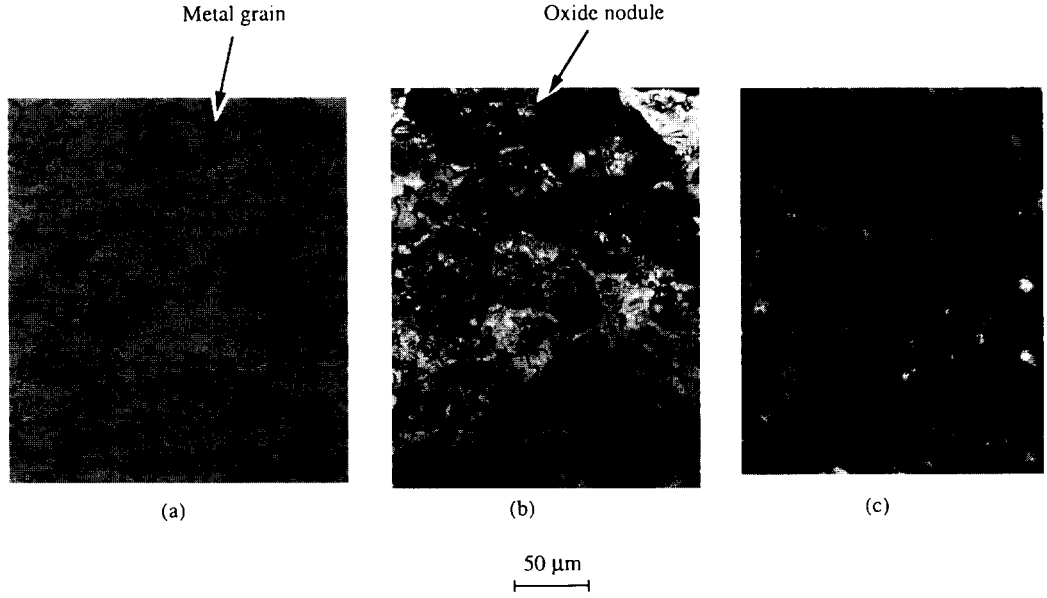

Fig. 2. Surface morphology of Zr/Zry/Zr disk specimen: (a) Before reaction; (b) after reaction, white oxide (OP67) and (c) after reaction, black oxide (OP65).

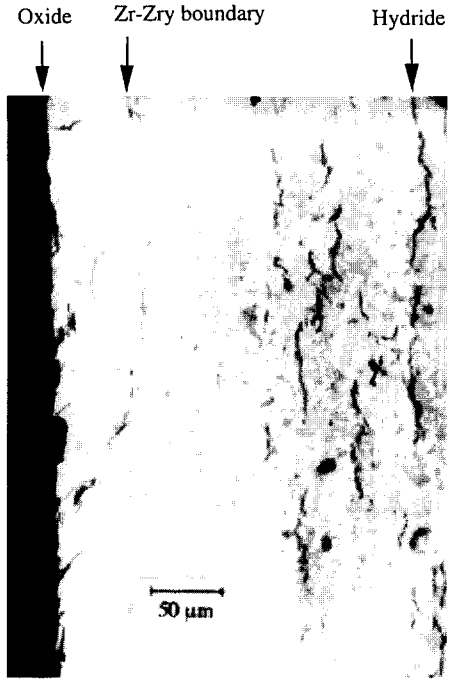

Fig. 3. Cross-section of Zr/Zry/Zr specimen oxidized for 47 h in 20% steam and 80% hydrogen at 400°C and 70 atm (disk center spot: OP62) (×280).

white oxide is cracked due to volume expansion. These white nodules are easily destroyed and leave dents during etching (see photo (b)).

Specimens oxidized at 350°C (Table 4) shows more uniform (black) oxide surfaces than those oxidized at 400°C (Table 5). Specimens with oxidation times longer than 24 h turned gray without visual white spots. This implies that increasing the oxidation temperature (from 350 to 400°C) increases the likelihood of producing white bumpy oxides. Since a thicker oxide is obtained at a higher temperature for a given oxidation time, this also suggests that increasing the oxidation time produces more white oxide.

3.2. Weight gain data

3.2.1. Correction for hydrogen absorption

In all tests utilizing H_2 as the carrier gas, the steam concentrations were above the critical values at which massive hydriding occurs ($\sim 0.5\%$ at 400°C and $\sim 0.02\%$ at 350°C, [25]). In gases with steam contents below the critical value, massive hydriding destroys the specimens within hours of initiation. Even for steam concentrations above the critical value, significant hydrogen absorption from the gas phase is observed. In this region, oxidation rates were calculated by correcting the weight gain for hydrogen absorption as determined by the hot-extraction method.

The oxidation rates in Tables 3–5 marked with 'a' were obtained by correcting for the weight gain due to hydrogen absorption. The typical weight gain contributions by hydrogen absorption are 14% for the oxidation rates in Table 3, 35% for Table 4 and 14% for Table 5. Therefore, the

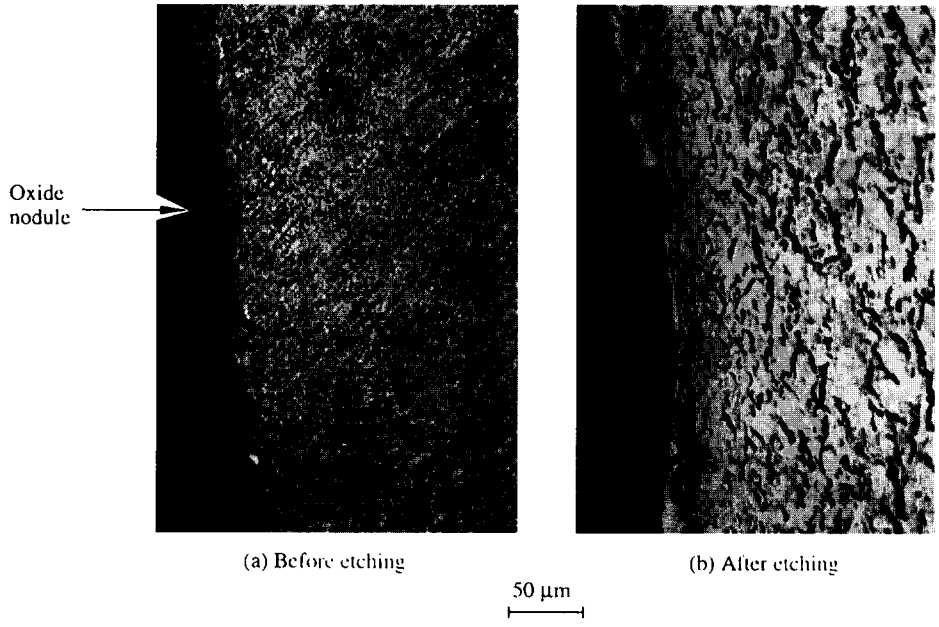

Fig. 4. Oxide morphology of Zr/Zry/Zr specimen oxidized in 1% steam and 99% hydrogen at 400°C and 70 atm (cross-section: OP67) (×280).

oxidation rates of specimens that were not analyzed for hydrogen are overestimated by these amounts.

3.2.2. Oxidation kinetics

The oxidation weight gains in 3% steam and 97% hydrogen mixture at 70 atm and 350°C (OP103) and 400°C (OP52) as functions of time are compared in Fig. 5. The initial ~ 3 h transient from the microbalance output on this figure is due to system stabilization (i.e., heat-up and pressurization of the system). The weight difference obtained by subtracting the initial value acquired by extrapolation of the linear curve to the weight axis from the final weight is ~ 15% smaller than the weight gain obtained by before-and-after measurements using the table-top microbalance. The discrepancy is believed to be due to the weight gain during the initial system stabilization period. As seen in the figure, the weight gains are linear function of time for two or three days although the initial oxidation kinetics is missing from the microbalance output. The linear behavior of weight gain versus time is also found in the long-term oxidation run (~ 6 days) shown in Fig. 6. The wavy microbalance output is not due to real weight changes. Rather the fluctuations are due to system instabilities such as temperature changes, pressure changes and natural circulation of the pressurized reacting gas in the specimen chamber. However, the long-term microbalance output fluctuates on the real weight changes. The slope of the straight line is drawn through the microbalance output in Fig. 5 represents real rate of weight change.

The totality of the oxidation rate data for sponge-Zr are displayed in Fig. 7. The data include the following conditions: (i) total gas pressures of 1 and 70 atm, (ii) temperatures of 350 and 400°C, (iii) steam concentrations greater than 1% and (iv) H_2 and He diluent gases. There is no systematic variation of the rate with any of above variables, and no case was significant deviation from linear kinetics observed in experiments lasting up to five days.

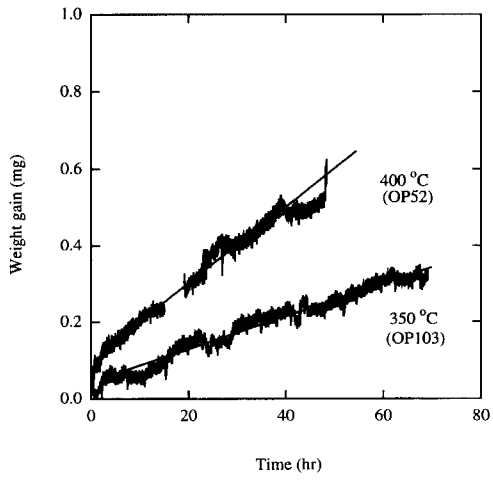

Fig. 5. Comparison of oxidation weight gain curves of Zr/Zry/Zr at 350 and 400°C in 5% steam and 95% hydrogen at 70 atm.

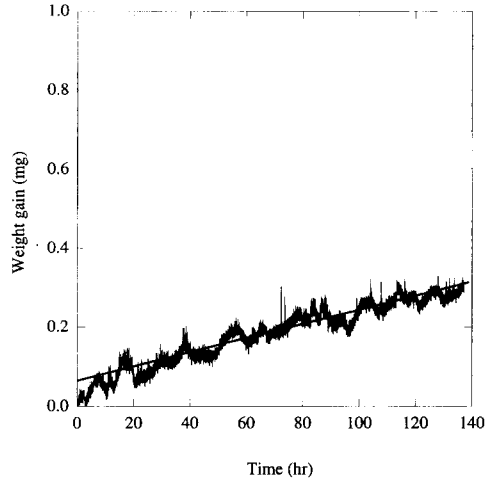

Fig. 6. Zr/Zry/Zr reaction in 0.5% steam and 99.5% hydrogen at 400°C and 70 atm (preoxidized film thickness = 2.9 μm) (Run OP53).

Two parameters that could potentially influence the oxidation kinetics were not varied: (i) iron content of the sponge-Zr, which was fixed at 215 ppm by weight and (ii) surface preparation, which was restricted to the pickling procedure described in Section 2.

At each temperature, the oxidation rate varied over a range of an order of magnitude. This deviation is far greater than the accuracy of the weight-gain measurements and is attributed to uncontrollable specimen-to-specimen differences. Chief among these are local variations in iron content and microstructure of the large, one-of-a kind Zr/Zry/Zr sandwich plate from which the specimens

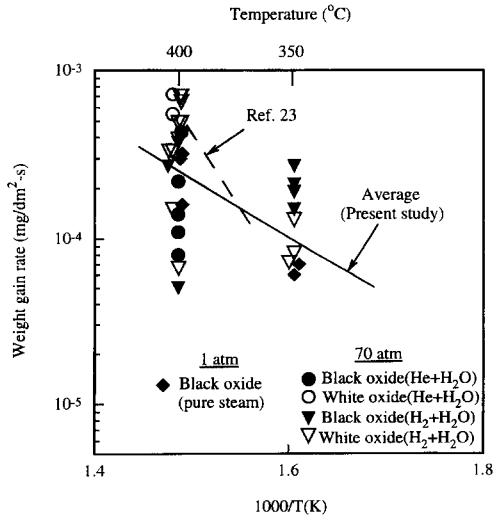

Fig. 7. Arrhenius plot of oxidation rates.

were cut. The line in Fig. 7 is drawn through the mid-range of the data band at each temperature and is given by the equation

$$\dot{w}\ (\mathrm{mg/dm^2\ s}) = 50\exp(-8200/T). \quad (1)$$

This line corresponds to an activation energy of ~ 16 kcal/mol, although this value is subject to considerable uncertainty arising from the variability of the data at the two temperatures investigated. At any temperature in this range, the oxidation rate is within a factor of ~ 2 of the value given by Eq. (1).

At 400°C, the specimens that exhibited visual white, bumpy post-test surfaces correlated with higher-than-average oxidation rates. The white oxide appears to develop with large weight gains. This may be due to oxide scale rupture due to volume expansion of the oxide, perhaps for the same reason that is responsible for transition from cubic to linear oxidation kinetics in waterside corrosion. The data at 350°C do not show a clear relationship of oxidation rate and scale coloration as do the 400°C data. This may be due to the slower rate of oxidation at the lower temperature, which allows more time for oxide and metal deformation to accommodate the volume change of the former without fracturing the oxide.

3.3. Variables affecting the oxidation rate

3.3.1. Steam content of gas

Tables 4 and 5 include the results both from batch experiments and single-specimen experiments. Oxidation rates obtained in batch experiments show good agreement with the single-specimen experiments and within the batch as well. Since the batch experiments used higher steam-content gas (greater than 4%) than the single-specimen tests, oxidation rates are independent of steam content, provided that it is greater than the critical value below which massive hydriding occurs.

3.3.2. Carrier gas (He or H_2)

Comparing 400°C oxidation rates from Table 3 (steam–helium mixtures) and Table 5 (steam–hydrogen mixtures) shows that oxidation rates are independent of the carrier gas, at least in tests lasting up to 2 –3 days. The frequency of appearance of white oxide morphology is higher in hydrogen–steam mixtures than in helium–steam mixtures (compare Tables 3 and 5). This suggests that white oxide formation is enhanced by hydrogen.

3.3.3. Total pressure

In Fig. 7, the oxidation rates from 1 atm tests and 70 atm tests are statistically indistinguishable. The distinct pressure dependence reported in Refs. [17,18] (see Table 1) for crystal-bar Zr at higher temperatures (> 450°C) may be due to higher hydrogen absorption and hydrogen-induced nodular corrosion at high pressure steam. These articles, however, did not report hydrogen contents in the specimens.

3.4. Hydrogen absorption during oxidation

The trend in hydrogen contents in Table 5 shows that the higher the steam content in hydrogen gas, the less the amount of hydrogen absorbed. The high hydrogen contents measured in specimens reacted in low-steam-content hydrogen gas imply that additional hydrogen from the gas phase is absorbed simultaneously with oxidation by-product hydrogen pickup. In other words, hydriding occurs when oxidation still progresses. Oxidation rates decrease as the steam content decreases below ~ 1 mol% at 400°C.

Hydrogen contents versus time from all tests with steam contents ranging from 0.5 to 20% are shown in Fig. 8. This plot shows that hydrogen absorption depends only on reaction time, although the data are not sufficient to describe the kinetics of this progress as a function of H_2 partial pressure and temperature. The majority of the points on this plot represent pickup fractions greater than unity.

3.4.1. Critical steam content

Obviously the oxidation rate must approach zero as the steam concentration does the same. At steam contents in H_2 less than a 'critical' value, oxidation ceases and massive hydriding becomes the dominant chemical reaction. The critical steam contents in the 70 atm hydrogen separating oxidation and hydriding are 0.5% at 400°C and 0.02% at 350°C, respectively. However, oxidation and hydriding are not clearly divided. Instead, these processes tend to overlap near the critical value [26].

3.4.2. He versus H_2 carrier gas

The pickup fractions greater than unity for experiments OP31 and OP32 conducted in the early-version TGA are abnormal. For those experiments were conducted in helium–steam mixtures. The reason for this is probably that the specimens absorbed gas phase hydrogen during the

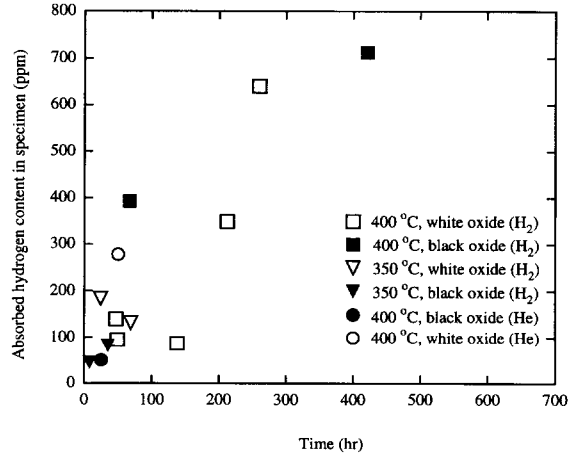

Fig. 8. Hydrogen absorption during oxidation of sponge-Zr by H_2–H_2O or He–H_2O mixtures (0.5–20 mol% steam).

initial stage of the experiments due to residual hydrogen in the apparatus. The hydrogen contamination was not large enough to affect oxidation kinetics. All runs except OP119 were obtained from the early-version TGA.

Specimen OP119 tested in the final-version TGA system shown in Fig. 1 exhibited a pickup fraction of 0.37, which is close to the normal value (~ 0.25). This experiment confirmed that the high pickup fractions of OP31 and OP32 were due to direct gas-phase absorption of residual hydrogen in the apparatus. Comparing the pickup fraction in run OP119 with those in Table 5 shows that hydrogen absorption is significantly higher in hydrogen–steam mixtures than helium–steam mixtures.

4. Conclusions

For temperatures between 350 and 400°C, the reaction of sponge Zr-coated Zry in mixed steam–hydrogen and steam–helium gases exhibits the following behavior.

(1) Two types of oxides are observed on sponge-Zr oxidized at 70 atm steam–hydrogen mixtures. One is black and uniform and the other white nodular. The black oxide film is fairly uniform. As the oxide thickens, white bumpy nodules are produced.

(2) Oxidation of sponge-Zr exhibits linear oxidation kinetics at least up to 5–6 days in 70 atm steam–hydrogen mixtures. The oxidation rate between 350 and 400°C has an activation energy of ~ 16 kcal/mol and is given by $\dot{w}(\mathrm{mg/dm^2\ s}) = 50\exp(-8200/T)$, where T in K.

(3) The oxidation rate of sponge-Zr is not dependent on steam concentration greater than 1% and is not dependent on the carrier gas (H_2 or He).

(4) The total pressure effect on oxidation is negligible.

(5) Gas phase hydrogen absorption from hydrogen–steam mixtures increases as the steam concentration approaches the critical H_2/H_2O ratio while oxidation progresses simultaneously.

References

[1] D.R. Olander, S. Vaknin, Secondary Hydriding of Defected Zircaloy-clad Fuel Rods, Electric Power Research Institute, EPRI TR-101773, 1993.
[2] H.S. Rosenbaum, et al., Large scale demonstration of barrier fuel, Proceedings of an International Symposium on Improvements in Water Reactor Fuel Technology and Utilization, IAEA-SM-288/30, International Atomic Energy Agency, 1987.
[3] C.J. Rosa, J. Less-Common Met. 16 (1968) 173.
[4] R.C. Nelson, The Corrosion of Zircaloy-2 Fuel Element Cladding in a Boiling Water Reactor Environment, GEAP-4089, 1962.
[5] W.E. Berry, React. Mater. 13 (1970) 44.
[6] E. Hillner, Corrosion of zirconium-base alloys: An overview, Zirconium in the Nuclear Industry, vol. 633, ASTM STP, 1977, p. 211.
[7] F. Garzarolli et al., Waterside corrosion of Zircaloy-clad fuel rods in a PWR environment, Zirconium in the Nuclear Industry, vol.754, ASTM STP, 1982, p. 430.
[8] T. Thorvaldsson et al., Correlation between 400°C steam corrosion behavior, heat treatment and microstructure of Zircaloy-4 tubing, Zirconium in the Nuclear Industry, vol. 1023, ASTM STP, 1989, p. 128.
[9] G.P. Sabol et al., Development of a cladding alloy for high burnup, Zirconium in the Nuclear Industry, vol. 1023, ASTM STP, 1989, p. 227.
[10] R.E. Westerman, High Temperature Oxidation of Zirconium and Zircaloy-2 in Oxygen and Water Vapor, HW-73511, 1962.
[11] N. Ramasubramanian, J. Electrochem. Soc. 128 (1981) 68.
[12] E.A. Gulbransen, K.F. Andrew, J. Electrochem. Soc. 4 (1966) 99.
[13] D. Weinstein, F.C. Holtz, Development of Improved Zirconium Alloys for use in Superheated Water and Steam, GEAP-4089, 1962.
[14] D.L. Douglass, The Metallurgy of Zirconium, IAEA, Suppl., International Atomic Energy Agency, Vienna, 1971.
[15] B. Cox, in: Oxidation of Zirconium and its Alloys, Advances in Corrosion Science and Technology, Vol. 5, eds. M.G. Fontana and R.W. Staehle (Plenum, New York, 1976).
[16] A.W. Urquhart et al., J. Electrochem. Soc. 125 (1978) 199.
[17] J.N. Wanklyn et al., J. Electrochem. Soc. 110 (1963) 856.
[18] B. Cox, The Effect of some Alloying Additions on the Oxidation of Zirconium in Steam, AERE-R 4458, 1963.
[19] R.E. Pawel et al., J. Nucl. Mater. 82 (1979) 129.
[20] D.W. Shannon, Corrosion 19 (1963) 414t.
[21] A.B. Johnson Jr., Corrosion and failure characteristics of zirconium alloys in high-pressure steam in the temperature range 400 to 500°C, Applications-related Phenomena for Zirconium and its Alloys, vol. 458, ASTM STP, 1969, p. 271.
[22] S. Kass, The development of the Zircaloys, Corrosion of Zirconium Alloys, vol. 368, ASTM STP, 1963, p. 3.
[23] A. Seibold et al., Nucl. News Apr. (1995) 36.
[24] Y.S. Kim et al., High Temp. High Pressures 27&28 (1995/1996) 55.
[25] D.R. Olander et al., Investigation of the roles of corrosion and hydriding of barrier cladding and fuel pellet oxidation in BWR fuel degradation, Proceedings of the 1997 International Topical Meeting on Light Water Reactor Fuel Performance, Portland, OR, 1997.
[26] D.R. Olander et al., Chemical Processes in Defective Fuel Rods, Electric Power Research Institute, EPRI TR-107074, Dec. 1996.